JOURNAL LA MULTIAPP

VOL. 05, ISSUE 05 (668-679), 2024
DOI: 10.37899/journallamultiapp.v5i5.1579

Analysis of Excavation Methods Against Deformation in Highway Tunnels

Dian Eka Aryanti[1], Singgih Saptono[2]

[1]*Bandung Energy and Mining Polytechnic, Indonesia*
[2]*Department of Mining Engineering, Faculty of Mineral Technology, UPN Veteran Yogyakarta*

**Corresponding Author: Dian Eka Aryanti*
Email: dianeka_aryanti@yahoo.com

Article Info

Article history:
Received 14 August 2024
Received in revised form 11 September 2024
Accepted 30 September 2024

Keywords:
Deformation
Excavation Method
Numerical Modelling
Length of Excavation

Abstract

Cisumdawu tunnel is a highway tunnelling which composed of very weak rock mass conditions has an average compressive strength less than 1 MPa. It is located below groundwater level. The shape of tunnell is horseshoe, diameter of tunnel section 14,413 m and height 11,083 m. Cisumdawu tunnel is a shallow tunnel which has a maximum overburden of 52,8 m and minimum overburden approximately 14 m. In the case of shallow tunnel which has a large section could be lead an instability during tunnel construction. Tunnel deformation analysis is using an observation and numerical modelling approach with finite element method which is assisted by RS 2019 (Rocscience) software. Based on the research is obtained that excavation method greatly affects the level of deformation that occurs during tunnel construction. As tunnelling advanced, Vertical displacement in the longitudinal direction using three bench seven step excavation method is smaller than full face and bench excavtion method. The maximum displacement using three bench excavation method is -4.23 mm, the full face method is -5.51 mm and the bench method is -4.91 mm. The amount of displacement is affected by the length of excavation and stage in tunnelling. The rate of deformation is increasing as the length of excavation getting deeper, but this is applied in unsupported tunnel.

Introduction

The Cisumdawu Tunnel is a highway tunnel that connects the Cisumdawu toll road which stretches from Bandung Regency (Cileunyi), Sumedang Regency and Majalengka Regency (Dawuan) with a length of 61.5 km. The Cisumdawu Tunnel is precisely located in Cilengger Village, Sumedang Regency, Bandung, West Java. The construction of the tunnel penetrates the hills, is a double tunnel that has a length of about 472 m in each tunnel. The Cisumdawu Tunnel is horseshoe-shaped with a diameter of 14,413 m and a height of 11,083 m. The Cisumdawu Tunnel has an average infill depth of less than 50 m, namely with a maximum height of 52.8 m and a minimum height of about 14 m. The condition of the rock mass in the tunnel is a very weak rock with an average compressive strength of less than 1 MPa. The construction of the Cisumdawu tunnel is located below the groundwater level. The excavation method used in the tunnel construction uses the New Austrian Tunnelling Method (NATM) method.

In the case of the Cisumdawu tunnel which is located relatively shallow, has a weak rock mass condition and large enough tunnel dimensions can cause large deformation during tunnel construction (Hung et al., 2009). Deformation that is too large due to tunnel excavation activities can cause collapse in the tunnel. For this reason, studies and analyses are needed to

ISSN: 2716-3865 (Print), 2721-1290 (Online)

determine the effect of tunneling activities on the magnitude of deformation that occurs so that control of deformation can be carried out (Hosseinitoudeshki, 2013).

Methods

There are many approaches in analyzing the deformation that occurs due to tunnel excavation, one of the methods that is often used is to use finite element numerical modeling. The analysis method in this study uses an approach through observation and numerical modeling with the finite element method (Mollon et al., 2009). The research methodology includes primary data collection and secondary data collection, as follows:

Data Collection in the Field

In the analysis of the facial stability of this excavation, data collection was carried out in the field, including primary and secondary data. Data collection taken in the field is in the form of:

Measurement of the strength of the rock mass at each excavation progress using *pocket penetrometer*. *Pocket penetrometer* designed as a lightweight instrument to be used to examine the visual classification of the soil (Yasun, 2018). Readings obtained from the penetrometer do not replace the results of laboratory tests. *Pocket penetrometer* It is spring operated, and measures the force with a direct reading scale in tons/sqft, or kg/cm^2 by pushing a piston with a diameter of 1/4in into the ground to a depth of 0.25 inches. The compression load is indicated by reading the scale on the piston barrel. The standards used in measurements using penetrometers are ASTM WK27337 *New Test Method for Pocket Penetrometer Test*.

Figure 1. Pocket Penetrometer

Measurements were made on the progress of the excavation, namely *bench* I, *bench* II and *bench* III . Measurements were carried out at 30 points on each *bench*.

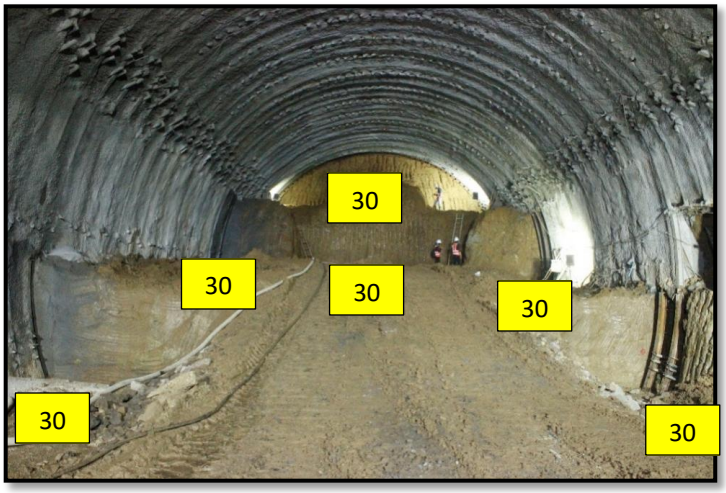

Figure 2. Illustration of Measurement Using Pocket Penetrometer on Bench I, II, and III

Sampling of rock masses. *Disturbed* samples were taken as many as 9 samples, with a total of 3 samples on each *bench* (Pan & Dias, 2017). The standard used in the sampling of

ISSN: 2716-3865 (Print), 2721-1290 (Online)

disturbed rocks in this rock mass is the AS standard 1289.1.2.1. Sampling was disrupted by the use of equipment in the form of shovels, aluminum foil, and plastic samples. Meanwhile, the collection of *undisturbed samples* was carried out according to the ASTM D-1587-83 standard using a standard steel tube (*shelby tube*) with a length of 50 cm and a diameter of 68 mm. UDS sampling was carried out at 3 points with a sampling distance of about 5 meters.

Shotcrete sampling with an age of 28 days, a height of 20 cm and a diameter of 7.5 cm was taken as many as 3 samples.

Grouting sampling with an age of 28 days, sample size of 5 x 5 cm as many as 3 samples.

Sample Testing in the Laboratory

The laboratory tests carried out are physical property tests and mechanical property tests. Physical property tests carried out using disturbed samples include:

Sieve analysis test with SNI 03-1968-1990 test standard, this test aims to obtain the distribution of the amount or percentage of grains both fine aggregate and coarse aggregate. This test was carried out on *disturbed samples* using scales and balancers, a set of filters, ovens, *dividers*, and brushes. Testing was carried out as many as 9 samples were disrupted.

Hydrometer test with SNI 03-3423-1994 test standard, which aims to obtain the amount from the distribution of soil grain size.

Moisture content test with SNI 1965:2008 test standard, the usefulness of the results of this moisture test can be applied to determine the consistency of material behavior and its properties, in cohesive soils soil consistency depends on the value of the moisture content. In addition, this moisture content value can also be used for other tests such as testing the determination of liquid limits and soil plastic limits.

Contents weight test using ASTM D1556 / D1556M standard, this test method is used to determine the density and content of compacted groundwater.

Testing of mechanical properties in the laboratory using UDS samples and buffer samples, including: 1) *Unconsolidated Undrained Triaxial Test* (Triaxial UU), the purpose of this test is to obtain the shear angle in the soil and cohesion. This test refers to the ASTM D-2850-87 standard; 2) *Consolidated Undrained Triaxial Test* (Triaxial CU), aims to obtain deep shear angles and ground cohesion both under total stress and effective stress conditions. The test procedure refers to the ASTM D-4767-88 standard; 3) Compressive strength testing *of* shotcrete *and* grouting *samples referring to ASTM C39/C 39 M standard to obtain compressive strength and buffer elastic modulus values.*

Secondary Data Capture

Secondary data collection includes tunnel geometry, namely tunnel width and height, length of excavation progress, *tunnel cross section* , topographic map, laboratory test results of rock mass characteristics and buffers

Research Approach and Methods

Numerical Modeling

In this method, tunnel excavation simulations are modeled and the tension and deformation conditions around the tunnel are analyzed using numerical modeling

Results and Discussion

Geology of the Cisumdawu Tunnel Area

Based on the results of geotechnical drilling at 8 drilling points, there are three types of rock units, namely at the initial depth consisting of a mixture of residual soil and *silty clay layers,*

ISSN: 2716-3865 (Print), 2721-1290 (Online)

sandy silt layers and *clayey* silt layers. At the initial depth of the mixture of residual soil with silty clay rock layers , it has characteristics of clay grain size to dark brown to reddish-brown silt, firm to rigid, there are rock fragments that are pebble-sized. The *sandy silt* rock layer has a yellowish-brown characteristic, has a grain size of sand to silt, there are rock fragments that are pebbles to shells, rock fragments are easy to detache from the matrix and decompose. The *clayey silt* layer is characterized by grayish-brown to blackish-gray color, there are rock fragments with a base mass that is still visible and is rigid to hard.

Observation activities in the field, the rock mass layer at the research site was deposited in harmony and no geological structure was found in the Cisumdawu tunnel. Figure 3 presents the results of the excavation face mapping at STA 12+750 in the Cisumdawu tunnel.

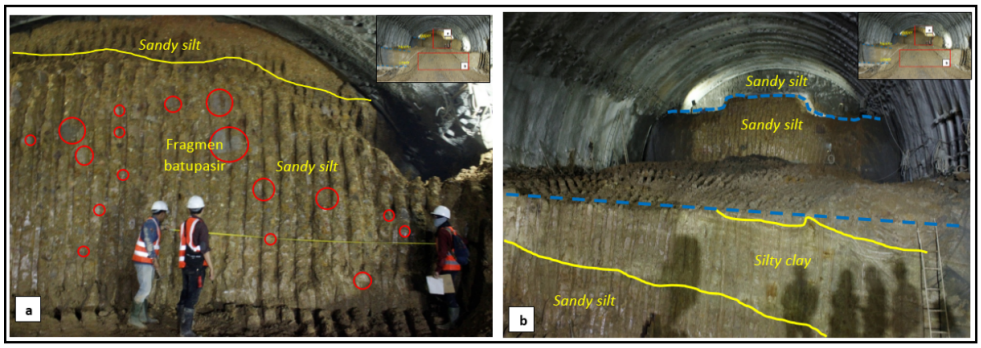

Figure 3. Excavation Face Mapping in the Cisumdawu STA 12+750 Tunnel (a) Sandy silt layer on the upper and core of the tunnel, dissemninated rock fragments on the core of the tunnel, (b) Sandy silt with silty clay inserts on the lower part of the tunnel excavation

Based on visual observations in the field, figure 3.1.a shows that the rock layer in the upper part of *the* tunnel excavation has a yellowish-brown color. The lithological contact between the rock layers could not be identified, based on the size of the grain being *sandy silt*. In the *core* there is material in the form of *sandy silt* with rock fragments in the form of gray sandstone and clay with a size of about < 50 cm. These rock fragments are relatively *rounded.* Based on the grain size in figure 3.1.a is a type of material deposition in the form of *fining upward*. In Figure 3.1.b, the *lower* part of the excavation is a layer of brownish *sandy silt* rock with an insert of a brownish-white *silty clay* layer. Field observations in the Cisumdawu Tunnel area based on *face mapping* data show that the rock mass layer in the tunnel is *sandy silt*.

Based on the results of the excavation face mapping, it was identified that it had a degree of weathering with class IV (BS 5930; 1981). The results of XRD testing conducted on 3 rock samples obtained the following results:

Deskripsi material	Komposisi mineral	Tingkat pelapukan
Berwarna coklat kekuningan, terdapat fragmen batuan berukuran kerikil, lapisan *sandy silt*	Magnetite, cristalobalite , halloysite, albite, ilite, nontronite	Tinggi (IV)
Berwarna coklat –coklat kekuningan, terdapat fragmen bps dan blp berukuran <50 cm, lapisan *sandy silt*	Halloysite, magnetite, cristalobalite, kuarsa	Tinggi (IV)
Berwarna kecoklatan, lapisan *sandy silt* dengan sisipan *silty clay* berwarna putih kecoklatan	Halloysite, magnetite, cristalobalite, kuarsa, ilite	Tinggi (IV)

Figure 4. Weathering Rate and Mineral Composition in the Cisumdawu Tunnel

ISSN: 2716-3865 (Print), 2721-1290 (Online)

The degree of weathering of igneous rocks, which is at Grade IV, indicates that most of the rock mass has turned into soil. Based on the results of XRD testing, there are secondary minerals in the form of clay minerals, namely ilite and nontronite, as well as halloysite. Halloysite is a type of secondary mineral that characterizes igneous rocks.

Characteristics of Rock Masses at the Research Site

SPT test can be used to distinguish the class of rock weathering (Lee et al., 2020; Ietto et al., 2016). At the research location, the average value of N SPT was 7.8% (N SPT >50) included in class B, 13.6% (N SPT 30-50) was included in class C, 58.4% (N SPT 10-30) was class D, and 20.8% (N SPT <10) was class E. The classification of the weathering class of rock masses based on the N-SPT value can be seen in Figure 4 below.

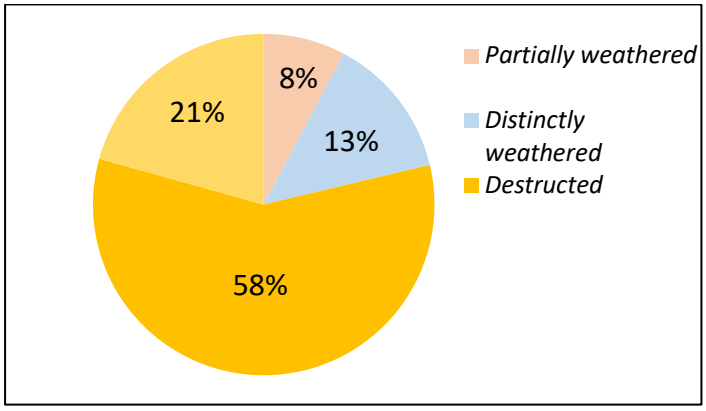

Figure 5. Classification of Rock Mass Weathering Class Based on N-SPT Value

The results of the analysis of the SPT test show that most of the rock mass layers at the research site have a high degree of weathering to completely *weathered*.

Based on the results of the penetrometer test, the classification of the strength of the rock layer at the research site consists of 3 (three) types, namely *medium stiff, very stiff,* and *hard.*

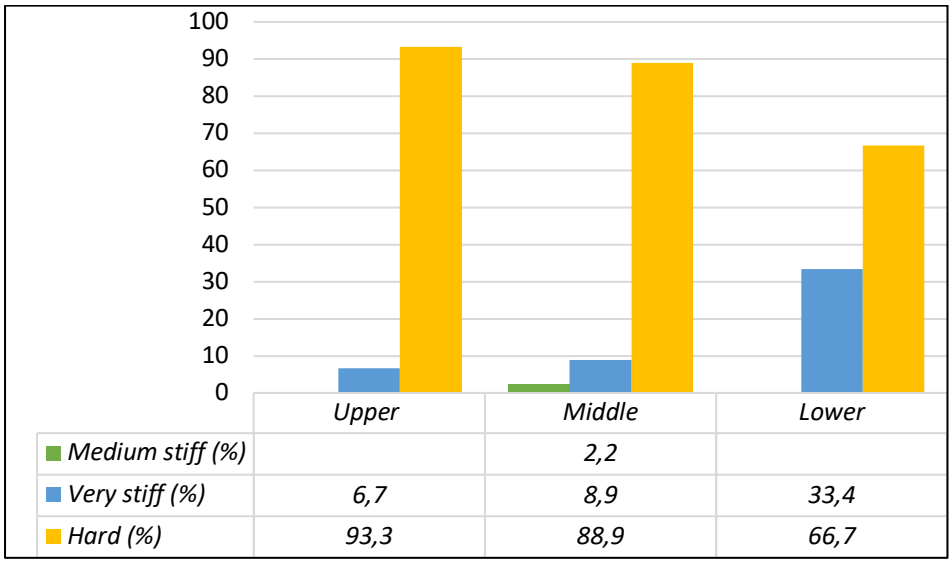

	Upper	Middle	Lower
Medium stiff (%)		2,2	
Very stiff (%)	6,7	8,9	33,4
Hard (%)	93,3	88,9	66,7

Figure 6. Percentage of Rock Layer Strength Based on Penetrometer Measurement Results In the Upper, Middle and Lower Tunnels

The results of the compressive strength test of rock masses carried out in the laboratory from 8 drilling points were 0.3 MPa to 1.2 MPa. Based on the classification of rock masses by ISRM (1981), it shows that the rock mass at the research site includes extremely weak rock R0 (*extremely weak rock*). The criteria for classifying rock mass were analyzed using the

ISSN: 2716-3865 (Print), 2721-1290 (Online)

results of field investigations, including elastic wave velocity (vp) testing and competency factors. The elastic wave speed (vp) at the research site ranged from 1.9 km/s to 2.4 km/s with a competency factor of 2.1 to 4.5. The classification of rock mass at the research site based on the value of elastic wave velocity and competency factors included in the DII rock mass class (Joshi, 2024).

The physical properties of the rocks at the research site are based on the results of laboratory tests from 8 (eight) drill points, including content weight, grain size, and plasticity index. The table below shows the average value of the properties in each layer of very weak rock.

Table 1. The physical properties of the rock layer are very weak

Rock Layers	**Contents weight (γn) (NM/m3)**	**Grain Size (%)**		**Plasticity Index (%)**		
		Sand	***Clay + Silt***	**WL**	**WP**	**IP**
Medium stiff silty clay	0,0166	21,57	78,43	65,79	37,82	27,97
Very stiff sandy silt	0,0162	36,91	63,09	61,79	38,07	23,72
Hard clayey silt	0,0161	27,39	72,61	72,28	42,83	29,44

Mechanical properties testing includes compressive strength testing (*unconfined compressive strength*) and triaxial testing. Compressive strength testing aims to classify the strength in rocks. Triaxial testing was carried out on an undisturbed sample taken at 3 points at STA 12+750. Triaxial testing aims to determine the mechanical properties of rocks in the form of cohesion and deep shear angle. The triaxial tests carried out include triaxial tests of the Law and CU based on the SNI 03-2815-1992 standard. The table below shows the results of triaxial testing on STA 12+750.

Table 2. Triaxial Test Results of Law and CU STA 12+750

UDS Sample Code	**Cohesion c**	**Sliding Angle in φ**
	(MPa)	(°)
STC UU 1	0,071	42,56
STC UU 2	0,079	28,88
STC CU	0,043	24,52

Numerical Modeling of the Cisumdawu Tunnel

Numerical modeling is carried out to provide an overview of the deformation that occurs in the tunnel. Numerical modeling is created in three dimensions using the help of RS 2019 software. Finite element method in 3D numerical modeling using RS 2019 (*Rocscience*) software. With the 3D finite element method, it is possible to simulate the tunneling process gradually (*sequential*), so that it can describe the 3D effect on different excavation methods. The dimensions of this 3D model are 176 m long, 96 m high and 50 m wide. In the design, the tunnel is modeled with a tunnel structure length of 16 m.

ISSN: 2716-3865 (Print), 2721-1290 (Online)

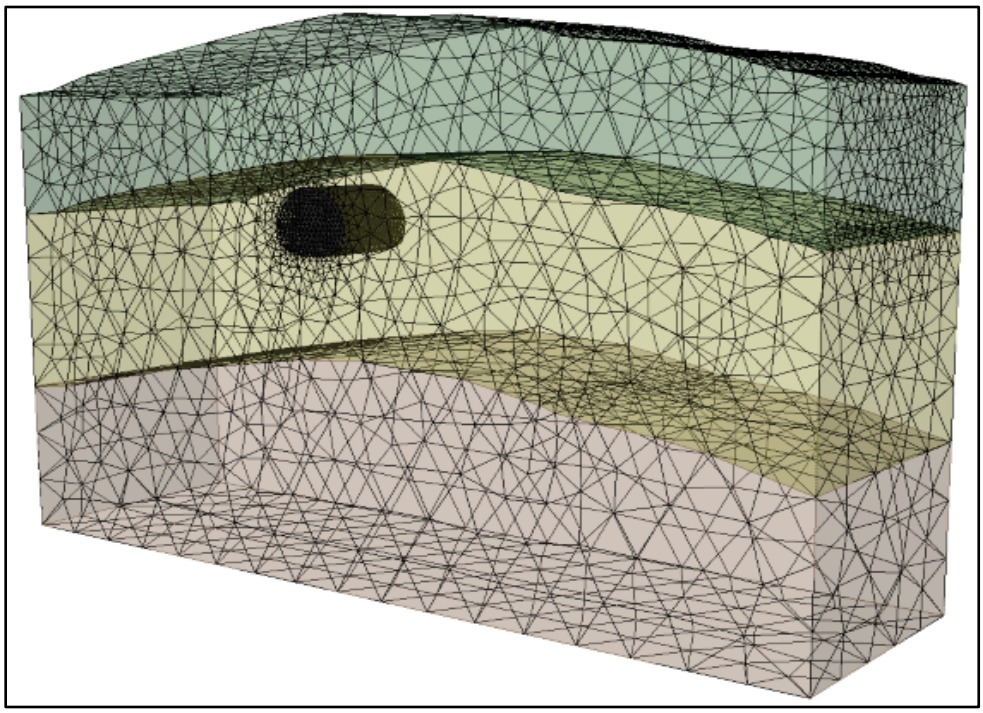

Figure 7. Geometry of 3D Numerical Modeling of Cisumdawu Tunnel

The boundary condition in numerical modeling serves to provide an assumption of the deformation value on the desired side, assuming that this boundary condition will affect the displacement value and the resulting force. The creation of boundary conditions in modeling is assumed not to be allowed to move on the horizontal axis. At the bottom of the horizontal and vertical axes are made fixed so that the model is made to remain in position after being loaded.

Tunnel geometry with isometric display has boundary conditions, namely *XYZ restrain* in XY plane, *XY restrain* in XZ and YZ planes, and on the surface is left free (*free restrain*).

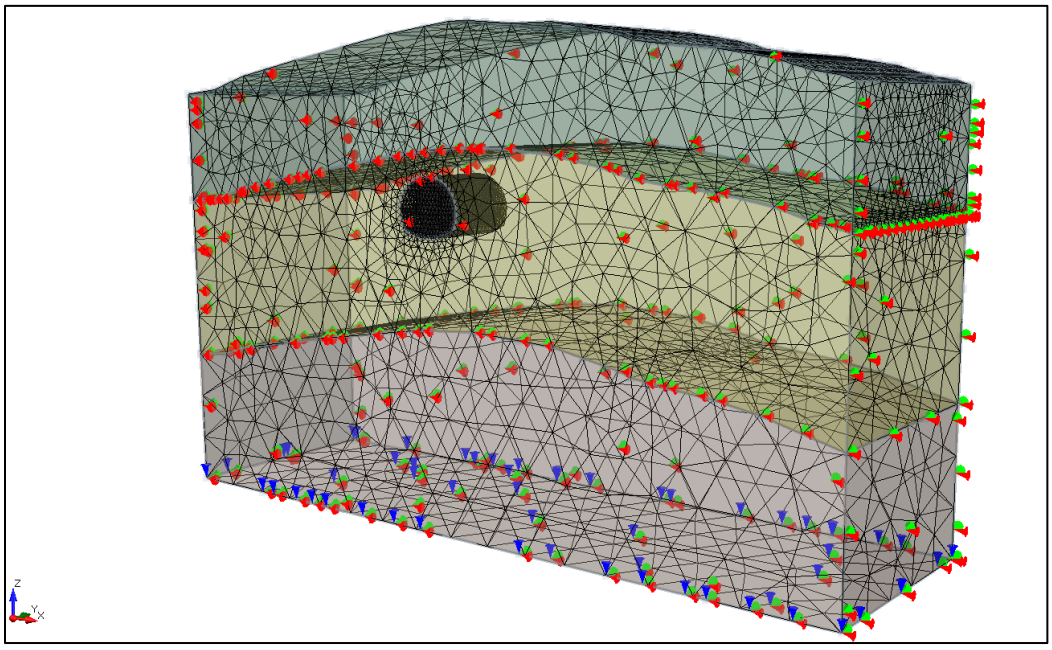

Figure 8. Boundary Conditions in 3D Modeling of Tunnels with Restrain Limits at XY and Fixed Restrain XYZ

ISSN: 2716-3865 (Print), 2721-1290 (Online)

Input parameters in the form of *field stress*, loading type, material type and mesh type as well as collapse criteria in numerical modeling simulation are presented in Table 3.

Table 3. Inputs in Numerical Modeling

Field stress	Gravity (actual ground surface)
Initial element loading	Field stress and body force
Failure criteria	Mohr-coulomb
Material type	Plastic (Peak = residue)
Mesh type	Graded with 4-noded triangles

The input parameters consist of material properties which include content weight, cohesion, deep shear angle, and modulus of elasticity as well as buffer properties in Table 4. and Table 6. as follows.

Table 4. Input Parameters on 3D Numerical Modeling

Parameters	Unit		L1	L2	L3
Filling weight	γn	MN/m3	0,018	0,0162	0,0161
Cohesion	c	Mpa	0,0379	0,0329	0,0413
Deep sliding angle	φ	°	10,73	21,78	18,84
Deformation modulus	E	Mpa	63,39	75,81	76,68
* L1 = *medium stiff silty clay,* L2 = *very stiff sandy silt,* L3 = *hard clayey silt*					

Table 5. Specification of Input Properties of Buffer in Cisumdawu Tunnel

Properties	Buffer Type					
	Steel pipe	Steel rib (H beam W150x18)	Wiremesh	SFRS	Concrete	Steel bar
E (MPa)	210000	210000	180000	26316	16666,67	210000
υ	0,25	0,25	0,25	0.28	0,3	0,25
T (MPa)	510	400	3	15,18	24.83	690

* E = modulus of elasticity, υ = poisson ratio, T = *tensile strength*, c = cohesion

Several model simulations were carried out to find out the deformation that occurred in different excavation methods. Based on the results of data processing in the previous chapter, it shows that the criteria for the rock mass class at the research site are included in *the extremely weak rock* category and according to JSCE (2007) the rock mass class is DII. The recommended excavation method based on the empirical approach of JSCE (2007) is a level excavation method. To determine the influence of the excavation method on the stability of the tunnel, an approach was carried out using numerical modeling so that the deformation value due to tunnel excavation can be predicted based on the total displacement and vertical displacement that occurs on the ground surface (Dias & Oreste, 2013; Zhang et al., 2013; Lin et al., 2024; Mu et al., 2021).

Tunnel Deformation Analysis to Excavation Method

In this study, a simulation of different tunnel excavation methods was carried out, namely *full face* and *bench method*. The deformation values that occur on the roof, walls and floor of the tunnel are analyzed using numerical modeling (Wang & Cai, 2022). Numerical modeling was carried out with a tunnel excavation depth of 16 m. The total displacement value in the longitudinal direction of each excavation method can be seen in Figure 9. as follows (Lunardi, 2008)

ISSN: 2716-3865 (Print), 2721-1290 (Online)

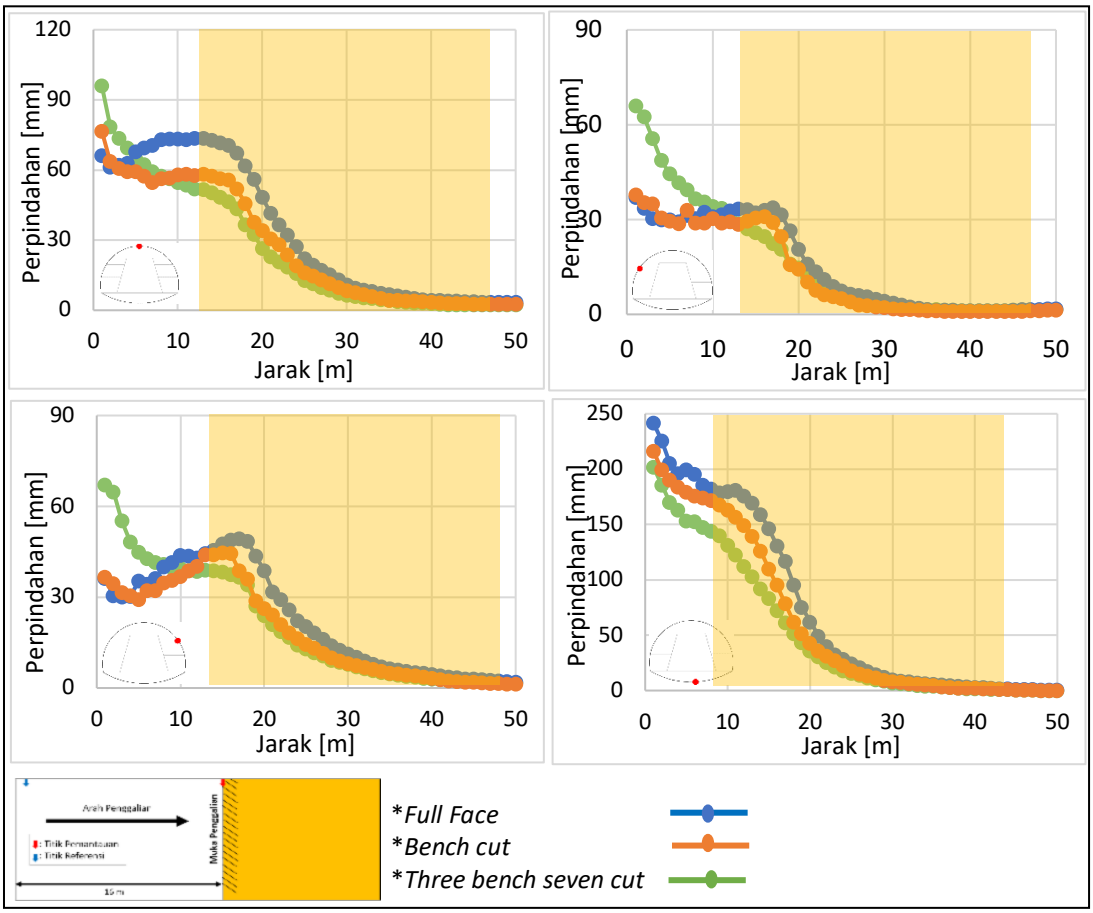

Figure 9. Total Displacement Value in Full Face and Bench Cut Excavation Method with Excavation Length of 16 m

Based on Figure 9, it can be seen if the displacement that occurs due to tunnel excavation with different excavation methods. In general, the displacement values on the roof, walls and floor of the tunnel show that the *three bench seven step* method produces a smaller deformation value compared to the other two methods (Ongodia, 2017; Sun et al., 2024; Song et al., 2020; An et al., 2024).

The vertical displacement that occurs on the ground surface due to excavation is analyzed through numerical modeling. The results of the analysis of subduction at the ground level in the simulation of *the full face* excavation method and *bench method* are presented in Figure 9. and Figure 10. as follows (Leca & Dormieux, 1990).

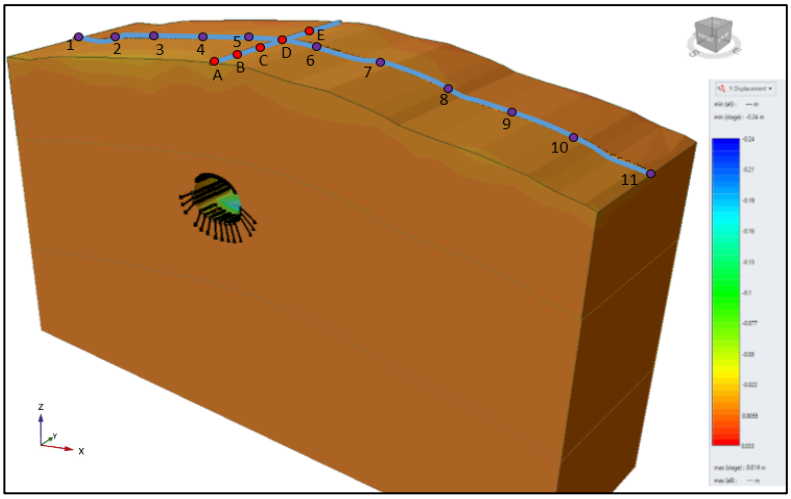

Figure 10. Vertical displacement observation point in 16 m tunnel excavation

ISSN: 2716-3865 (Print), 2721-1290 (Online)

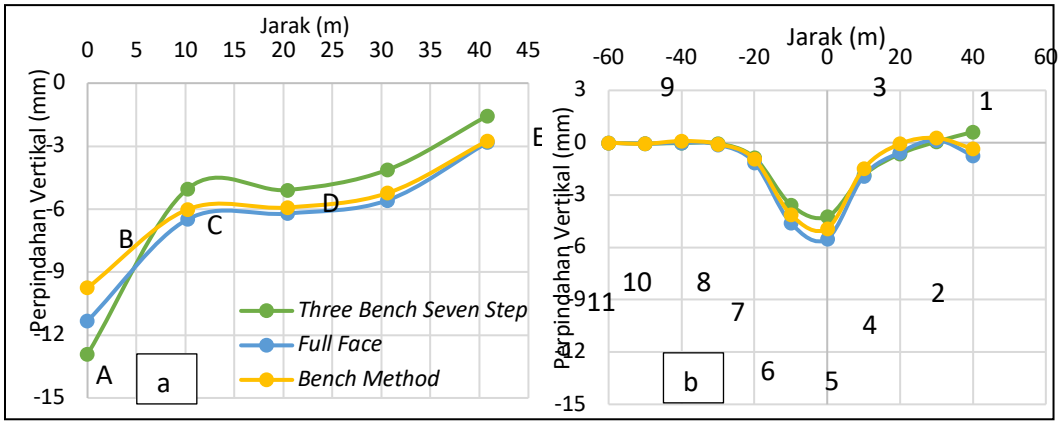

Figure 11. Displacement Prediction Based on Numerical Modeling

(a) Longitudinal Vertical Displacement (A-E), (b) Transverse Vertical Displacement (1-11)

The results of vertical displacement prediction through numerical modeling in Figure 11. Above shows that excavation using *the Three Bench Seven Step* method experiences a relatively smaller displacement compared to other excavation methods. Observations at 5 (five) longitudinal points, namely A, B, C, D, and E, show that the maximum vertical displacement occurs at observation point A located at the beginning of the tunnel excavation. The maximum vertical displacement value in the *three bench seven step* excavation method was -12.9 mm, *full face* -11.3 mm, and *bench method* -9.8 mm. Along with the progress of excavation, the *three bench seven-step* excavation method produces a smaller vertical displacement value in the longitudinal direction compared to other methods. Observations at 11 points in the transverse direction also show that the vertical displacement in the *three bench seven-step excavation method* is smaller than other methods (Niedbalski et al., 2018; Nie et al., 2024). The value of vertical displacement in the transverse direction reaches the maximum when passing through the tunnel excavation, which is at observation point 5. The maximum displacement value in the *three bench seven step* method was -4.23 mm, in the *full face* excavation method -5.51 mm, and in the *bench cut* excavation method -4.91 mm. The largest vertical displacement value occurs in the *full-face excavation method*.

Conclusion

The excavation method greatly affects the level of deformation that occurs in the tunnel. Along with the progress of excavation, the three bench seven-step excavation method produces a smaller vertical displacement value in the longitudinal direction compared to the full face and bench methods. The maximum displacement value in the three bench seven step method was -4.23 mm, in the full face excavation method -5.51 mm, and in the bench cut excavation method -4.91 mm. The largest vertical displacement value occurs in the full-face excavation method. The magnitude of the displacement is affected by the length of the excavation and the stages of excavation in the tunnel. The level of deformation increases as the length of the excavation gets deeper, but this is true when the tunnel has not been supported. The excavation stage that greatly affects the level of tunnel deformation is during the invert excavation stage (stage 7). The deformation rate decreases when the primary lining has been applied to the invert excavation.

References

An, Z., Ma, W., Wang, Y., & Yuan, Z. (2024). Stability analysis of extra-large-span tunnels during construction: a case study. *Geotechnical and Geological Engineering*, 1-15. https://doi.org/10.1007/s10706-023-02719-8

ISSN: 2716-3865 (Print), 2721-1290 (Online)

Dias, D., & Oreste, P. (2013). Key factors in the face stability analysis of shallow tunnels. *American Journal of Applied Sciences*, *10*(9), 1025–1038. https://dx.doi.org/10.3844/ajassp.2013.1025.1038

Hosseinitoudeshki, V. (2013). *Numerical analysis of K0 to tunnels in rock masses exhibiting strain-softening behaviour (case study in Sardasht dam tunnel, NW Iran).*

Hung, C. J., Wisniewski, J., Monsees, J., & Munfah, N. (2009). *Technical manual for design and construction of road tunnels-civil elements*. National Highway Institute (US).

Ietto, F., Perri, F., & Cella, F. (2016). Geotechnical and landslide aspects in weathered granitoid rock masses (Serre Massif, southern Calabria, Italy). *Catena*, *145*, 301-315. https://doi.org/10.1016/j.catena.2016.06.027

Joshi, P. C. (2024). Comparative Study of Rock Mass Classification Systems: A Case Study of Nagdhunga-Naubisea Road Tunnel. *Himalayan Journal of Applied Science and Engineering*, *4*(2), 1-10. https://doi.org/10.3126/hijase.v4i2.62183

Leca, E., & Dormieux, L. (1990). Upper and lower bound solutions for the face stability of shallow circular tunnels in frictional material. *Géotechnique*, *40*(4), 581–606. https://doi.org/10.1680/geot.1990.40.4.581

Lee, S. H., Baek, S. H., Woo, S. I., & Chung, C. K. (2020). Estimation of in situ geotechnical properties on highly weathered granite using chemical weathering indices. *Bulletin of Engineering Geology and the Environment*, *79*, 3403-3415. https://doi.org/10.1007/s10064-020-01771-5

Lin, Q., Meng, X., Lu, D., Miao, J., Zhao, Z., & Du, X. (2024). A unified empirical method for predicting both vertical and horizontal ground displacements induced by tunnel excavation. *Canadian Geotechnical Journal*. https://doi.org/10.1139/cgj-2023-0519

Lunardi, P. (2008). *Design and construction of tunnels: Analysis of Controlled Deformations in Rock and Soils (ADECO-RS)*. Springer Science & Business Media.

Mollon, G., Dias, D., & Soubra, A.-H. (2009). Probabilistic analysis and design of circular tunnels against face stability. *International Journal of Geomechanics*, *9*(6), 237–249. https://doi.org/10.1061/(ASCE)1532-3641(2009)9:6(237

Mu, B., Xie, X., Li, X., Li, J., Shao, C., & Zhao, J. (2021). Monitoring, modelling and prediction of segmental lining deformation and ground settlement of an EPB tunnel in different soils. *Tunnelling and Underground Space Technology*, *113*, 103870. https://doi.org/10.1016/j.tust.2021.103870

Nie, J., He, C., Kou, H., Liu, F., & Yang, W. (2024). Research on Excavation Method for Soft Rock Tunnel Based on Stress Release Rate. *Applied Sciences*, *14*(2), 668. https://doi.org/10.3390/app14020668

Niedbalski, Z., Małkowski, P., & Majcherczyk, T. (2018). Application of the NATM method in the road tunneling works in difficult geological conditions–The Carpathian flysch. *Tunnelling and Underground Space Technology*, *74*, 41–59. https://doi.org/10.1016/j.tust.2018.01.003

Ongodia, J. E. (2017). *Geotechnical engineering design of a tunnel support system-a case study of Karuma (600MW) hydropower project*.

Pan, Q., & Dias, D. (2017). Upper-bound analysis on the face stability of a non-circular tunnel. *Tunnelling and Underground Space Technology*, *62*, 96–102. https://doi.org/10.1016/j.tust.2016.11.010

ISSN: 2716-3865 (Print), 2721-1290 (Online)

Song, Z., Shi, G., Zhao, B., Zhao, K., & Wang, J. (2020). Study of the stability of tunnel construction based on double-heading advance construction method. *Advances in Mechanical Engineering*, *12*(1), 1687814019896964. https://doi.org/10.1177/1687814019896964

Sun, Y., Xu, S., Xu, C., Huang, W., He, J., Rong, Y., ... & Ding, L. (2024). Study on the Stress and Deformation of Surrounding Rock and Support Structure of Super Large Section Tunnels Based on Different Excavation Methods. *Applied Sciences*, *14*(16), 7025. https://doi.org/10.3390/app14167025

Wang, M., & Cai, M. (2022). Numerical modeling of stand-up time of tunnels considering time-dependent deformation of jointed rock masses. *Rock Mechanics and Rock Engineering*, *55*(7), 4305-4328. https://doi.org/10.1007/s00603-022-02871-2

Yasun, A. S. (2018). Capability of pocket penetrometer to evaluate unconfined compressive strength of baghdad clayey soil. *Al-Nahrain Journal for Engineering Sciences*, *21*(1), 66–73. https://doi.org/10.29194/NJES21010066

Zhang, Z., Huang, M., & Wang, W. (2013). Evaluation of deformation response for adjacent tunnels due to soil unloading in excavation engineering. *Tunnelling and Underground Space Technology*, *38*, 244-253. https://doi.org/10.1016/j.tust.2013.07.002

ISSN: 2716-3865 (Print), 2721-1290 (Online)